Searching for dark matter annihilating into light long-lived mediators from stars inside dwarf spheroidal galaxies

Aman Gupta,[1,2,*] Pooja Bhattacharjee,[3,†] and Pratik Majumdar[1,2,‡]

[1]*Theory Division, Saha Institute of Nuclear Physics, I/AF, Bidhannagar, Kolkata 700064, India*
[2]*Homi Bhabha National Institute, Anushakti Nagar, Mumbai 400094, India*
[3]*Center for Astrophysics and Cosmology, University of Nova Gorica, Vipavska 13, SI-5000 Nova Gorica, Slovenia*

(Received 21 January 2025; accepted 12 May 2025; published 2 June 2025)

Several astrophysical and cosmological observations suggest the existence of dark matter (DM) through its gravitational effects, yet its nature remains elusive. Despite the lack of DM signals from direct detection experiments, efforts continue to focus on the indirect detection of DM from DM-rich astrophysical objects. Dwarf spheroidal galaxies (dSphs) are among the most promising targets for such searches. In this work, we aim to investigate the expected DM capture rate from the stellar component of ten nearby DM-rich dSphs, assuming that the accumulated DM eventually annihilates into light, long-lived mediators (LLLMs) which decay into gamma rays outside the dSphs. We analyze nearly 16 years of *Fermi*-LAT data to search for DM annihilation through LLLMs, and, from the observed stacked flux upper limits, set limits on the DM-nucleon scattering cross section for the case of a generic DM scenario. Additionally, we incorporate the Sommerfeld enhancement (SE) effect into the DM annihilation process assuming a scalar DM model, and obtain bounds on the DM-nucleon scattering cross section of $\sim 10^{-36}$ cm^2 for DM masses around 100 GeV. This allows us to explore an alternative avenue for exploring DM phenomena from dSphs and compare our results with the bounds reported by direct DM detection experiments and other celestial bodies.

DOI: 10.1103/lg3d-fh1y

I. INTRODUCTION

Dwarf spheroidal galaxies (dSphs) are among the faintest, most dark matter (DM)-dominated galaxies in the Universe [1–4]. These small, low-luminosity systems, often found as satellites orbiting larger galaxies like the Milky Way, are characterized by an unusually high mass-to-light ratio, indicating a significant amount of DM relative to visible matter. Their lack of gas and star formation makes dSphs valuable targets for indirect DM detection, as this absence of astrophysical activity creates a relatively clean environment with minimal background noise [3,5]. The DM content in dSphs is inferred from the velocity dispersion of their stars [6], suggesting that the gravitational influence of unseen mass is substantial. Consequently, dSphs are promising candidates for searches aimed at detecting potential signals from DM annihilation or decay processes.

In indirect detection, dSphs are particularly valuable for gamma-ray searches because of their proximity and dense DM halos. Gamma rays, especially within the energy range of interest and resulting from DM annihilation, are of particular significance because they are electrically neutral, allowing them to travel directly from their source without being affected by Galactic or extragalactic magnetic fields, thus preserving information about their origin. The gamma-ray space telescope like the Fermi Large Area Telescope (*Fermi*-LAT) has conducted extensive searches for gamma-ray emissions from dSphs to constrain the DM annihilation cross section [7–17]. While no conclusive signals have yet been detected, the clean astrophysical environment of dSphs reduces the risk of false positives due to background contamination, making these galaxies ideal for setting stringent bounds on DM models and advancing our understanding of this elusive component of the universe.

Most studies on DM signal from dSphs establish upper bounds on the thermally averaged DM annihilation cross section [18–23], making comparisons with direct detection challenging. This study, however, explores a distinctive mechanism: we investigate DM annihilation into light long-lived mediators (LLLMs) that decay into gamma rays outside the galaxies, allowing us to constrain the DM-nucleon scattering cross section as a function of DM mass. The minimum detectable DM mass from celestial bodies and dSphs is governed by the DM evaporation rate, setting a limit on sensitivity in both indirect and direct detection approaches. This mechanism has been developed under

*Contact author: aman.gupta@saha.ac.in
†Contact author: pooja.bhattacharjee@ung.si
‡Contact author: pratik.majumdar@saha.ac.in

secluded DM models [24,25], which naturally predict the existence of LLLMs [26]. Theoretically, such particles are well motivated [27–30] and are actively being searched for in collider and fixed-target experiments [31–34]. Numerous works have considered LLLM scenarios in indirect detection (e.g., [29,30,35–43]). In particular, LLLMs have been invoked to explain the observed excesses in cosmic-ray electrons and positrons, as discussed in Refs. [44–46]. Reference [25] further shows that LLLM scenarios can enhance the DM annihilation rate, leading to stronger indirect detection signals. Various astrophysical objects have been considered as potential probes of secluded DM and LLLMs, including the Sun [36,38,39], Jupiter [47,48], the Earth [49], as well as brown dwarfs (BDs) and neutron stars (NSs) [50,51]. Yet our approach combines this with the inclusion of the Sommerfeld effect, which enhances annihilation rates at low velocities, providing a boost to the DM signal. Sommerfeld enhancement (SE) is the widely discussed phenomenon in the context of DM annihilation [21,45,52–54]. The authors in [20] explored the effects of SE on the DM annihilation cross section in dSphs using *Fermi*-LAT data. Reference [52], for instance, considers a combined effect of resonant annihilation and SE in the Standard Model (SM) Higgs portal and MSSM-inspired DM scenarios.

In this work, to the best of our knowledge, for the first time, we investigate the expected DM capture rate within the stellar component of ten nearby dSphs, hypothesizing that captured DM annihilates into LLLMs. Later we also incorporate the Sommerfeld effect in this framework considering a particular scalar DM model interacting with the scalar mediator.[1] Using nearly 16 years of *Fermi*-LAT gamma-ray data, we set upper limits on the gamma-ray flux and refine constraints on the DM-nucleon scattering cross section. This complementary method broadens traditional indirect detection approaches by focusing on stellar capture and mediator decay scenarios, offering a new avenue for probing DM interactions in dSphs.

We organize the paper in the following manner. Section II begins with a brief discussion about the choice of our selected dSphs, listing their important properties used in this work. Section III deals with the *Fermi*-LAT data analysis of the selected dSphs and calculation of gamma-ray flux upper limits. The formalism for DM capture and annihilation via LLLM from dSphs and the estimation of the gamma-ray spectrum from such processes have been reviewed in Secs. IV and V. In Sec. VI, we derive the constraints on DM-nucleon scattering cross section using *Fermi*-LAT observational data. Section VIII explores the simple model of the SE along with the decay of the LLLM, ϕ, into gamma rays. Finally, in Sec. IX, we conclude with a summary and prospect for future studies.

[1]In the first part of this work, we derive bounds on DM-nucleon scattering cross section without assuming any specific particle nature of DM and thus refer to these bounds as "model independent." In the second part, we incorporate the Sommerfeld enhancement (SE), which depends on the details of the DM model. For this (SE) case, we consider a scalar DM model, making our results model dependent. Please note that in both cases (with and without SE) the mediator is taken to be a scalar particle, which subsequently decays into gamma photons to produce observable signals.

II. OUR TARGETS: NEARBY DSPHS

The Milky Way hosts a large population of dSphs, which are small, faint, and have minimal star formation activity compared to larger galaxies. These dSphs are highly DM dominated, evidenced by their high mass-to-light ratios, and often embedded within extended DM halos. Their simple structure and relatively low baryonic content make dSphs ideal laboratories for studying DM properties because the effects of DM are less contaminated by stellar and gas dynamics. Given their proximity and abundance in the Milky Way, these halos provide an accessible means to examine DM interactions, including capture rates by stars within dSphs. By analyzing how DM might accumulate in stars, we can infer properties about DM particle interactions, helping to constrain models of DM capture and potentially shine a light on the nature of DM particles.

In this study, we are interested in assessing the potentiality of dSphs in constraining the DM parameter space under the mechanism where DM annihilates through the decay of intermediate particles, as mentioned above. In this regard, we restrict ourselves to only those dSphs whose distance from the Milky Way is less than 50 kpc which corresponds to only ten nearby dSphs (Table I), as the flux falls with distance ($\propto 1/d^2$).

In Table I, we describe the characteristic of our selected dSphs as follows: columns I and II: right ascension (RA) and declination (DEC) of our targets in degree; column III: heliocentric distance (d) in kpc; column IV: stellar radius ($R_\star$) in pc; column V: velocity dispersion ($\sigma_{\rm l.o.s}$) in km/s; and column VI: total stellar mass ($M_{\star,\rm tot}$) in unit $M_\odot$. We calculate the stellar radius $R_\star$ and $M_{\star,\rm tot}$ in Sec. IV following Ref. [55]. To estimate $M_{\star,\rm tot}$ and $R_\star$, we take the values of $N_{\rm tot}$ from Table 3 of [55] except for Sagittarius (Sgr) and Carina II cases for which we use the approximate values of total stellar mass reported in [56]. The values of other parameters such as RA, DEC, d, and $\sigma_{\rm l.o.s}$ are taken from [57,58] unless indicated in Table I. This Table also mentions the astrophysical uncertainties corresponding to the relevant dSph parameters d and $\sigma_{\rm l.o.s}$.

III. *FERMI*-LAT DATA ANALYSIS FOR DSPHS

A. Data selection

We analyze nearly 16 years of *Fermi*-LAT data, spanning from August 4, 2008, to June 2, 2024. For our analysis, we utilize Fermipy version 1.1.0 and Fermi ScienceTools version

TABLE I. Properties of our selected dSphs. Please see the text for more details.

Source	RA [deg]	DEC [deg]	d (kpc)	R_* (pc)	$\sigma_{\mathrm{l.o.s}}$ (km/s)	$M_{*,\mathrm{tot}}$ ($M_\odot$)
Draco II	238.17	64.58	$21.57^{+50}_{-0.49}$	13.03	< 5.9	30 [55]
Segue I	151.75	16.08	$22.90^{+2.21}_{-2.01}$	15.33	$3.7^{+1.4}_{-1.1}$	220 [55]
Sagittarius	283.83	−30.55	$26.30^{+1.88}_{-1.75}$	1199.45	$11.4^{+0.7}_{-0.7}$	21×10^6 [56]
Hydrus I	37.39	−79.31	$27.54^{+0.51}_{-0.50}$	40.62	$2.7^{+0.51}_{-0.43}$	3.0 [55]
Reticulum II	53.92	−54.05	$31.62^{+1.49}_{-1.42}$	23.76	$3.6^{+1}_{-0.7}$	764.0 [55]
Ursa Major II	132.87	63.13	$34.67^{+2.13}_{-2.01}$	65.15	$6.7^{+1.4}_{-1.4}$	296.0 [55]
Carina II	114.11	−58.0	$37.39^{+0.39}_{-0.39}$	59.01	$3.4^{+1.2}_{-0.8}$	0.38×10^6 [56]
Bootes II	209.51	12.86	$41.68^{+1.16}_{-1.13}$	29.89	$2.9^{+1.6}_{-1.2}$	298.0 [55]
Willman I	162.34	51.05	$38.01^{+7.68}_{-6.39}$	15.33	$4^{+0.8}_{-0.8}$	455.0 [55]
Coma Berenices	186.75	23.91	$42.26^{+1.58}_{-1.52}$	43.68	$4.6^{+0.8}_{-0.8}$	1307.0 [55]

2.2.0.[2] The data is processed with the source class instrument response function P8R3_SOURCE_V3.[3]

B. Analysis technique and gamma-ray flux upper limits

We focus on the energy range $E \in [0.5, 500]$ GeV and extract data within a 15° region of interest (ROI) centered on each dSph location. Our "source model" includes the "source of interest" along with all sources within the 15° ROI from the 4FGL-DR4 catalog [59].[4] Additionally, we incorporate the galactic diffuse model (gll_iem_v07.fits) and the isotropic diffuse model (iso_P8R3_SOURCE_V3_v1.txt).[5] After constructing the source model and generating all necessary input files, we perform a bin-by-bin binned likelihood analysis[6] on the extracted data. During this analysis, the spectral parameters of all sources within a $10° \times 10°$ ROI and the normalization parameters for the two diffuse background models are allowed to vary freely.

We model the gamma-ray emission from each dSph as a new pointlike source, assuming a power-law spectrum, $\mathrm{d}N/\mathrm{d}E \propto E^{-\Gamma}$, with a spectral index $\Gamma = 2$. To search for evidence of excess emission from the dSph location, we calculate the test statistic (TS), defined as $\mathrm{TS} = -2\ln(L_{\mathrm{max},0}/L_{\mathrm{max},1})$, where $L_{\mathrm{max},0}$ and $L_{\mathrm{max},1}$ are the maximum likelihood values for the null hypothesis (background only) and the alternative hypothesis (including the additional source), respectively. No significant excess emission is detected at any dSph location, with TS values falling well below the point source detection threshold of $\mathrm{TS} = 25$.

In the absence of excess emission, we calculate the 95% confidence level (CL) upper limits on the gamma-ray flux for each dSph using the profile likelihood method [60]. In this approach, the fit is performed until the difference in the log-likelihood function, $-2\Delta\ln(\mathcal{L})$, reaches 2.71, corresponding to the one-sided 95% CL.

In Fig. 1, we show the observed bin-by-bin $E^2\mathrm{d}\Phi/\mathrm{d}E$ flux upper limits for all ten dSphs considered in this work.

IV. FORMALISM FOR GAMMA-RAY FLUX CALCULATION VIA LLLMS FROM STARS INSIDE DSPHS

In this section, we present the key formulas and assumptions necessary to calculate the gamma-ray flux resulting from the two-step cascade annihilation of DM particles. We consider a scenario in which DM is captured by stellar components of dSphs in sufficient quantities, primarily through the scattering of nucleons. This interaction causes DM to lose kinetic energy and become gravitationally bound to the dSph. If accumulated in considerable amounts, such DM particles undergo self-annihilation producing gamma rays. It should be noted that in the two-step annihilation process, the DM particles first annihilate into LLLMs which later decay into gamma rays.

A. DM capture inside the stars of dSphs

DM, when traversing through celestial objects, undergoes single or multiple scattering with nucleons depending on the kinetic energy of DM. In due time, this process leads to their thermalization and eventual capture when their velocity falls below the escape velocity of dSph.

It should be noted that, in dense stellar environments stars such as neutron stars or white dwarfs, the stellar density, $\rho_*(r)$, is extremely high. In contrast, dSphs present a different scenario, as the majority of their mass resides in DM rather than baryons. Thus, to treat dSph, we need to account for the fact that: (i) the dSph galaxies have a very low baryon-to-DM ratio, and (ii) the nucleon density in dSphs is primarily from old stars with minimal contributions from gas or dust. These factors may produce enough DM interactions in the

[2] https://fermi.gsfc.nasa.gov/ssc/data/analysis/software/
[3] https://fermi.gsfc.nasa.gov/ssc/data/analysis/documentation/Pass8_usage.html
[4] https://fermi.gsfc.nasa.gov/ssc/data/access/lat/14yr_catalog/
[5] https://fermi.gsfc.nasa.gov/ssc/data/access/lat/BackgroundModels.html
[6] https://fermi.gsfc.nasa.gov/ssc/data/analysis/scitools/binned_likelihood_tutorial.html

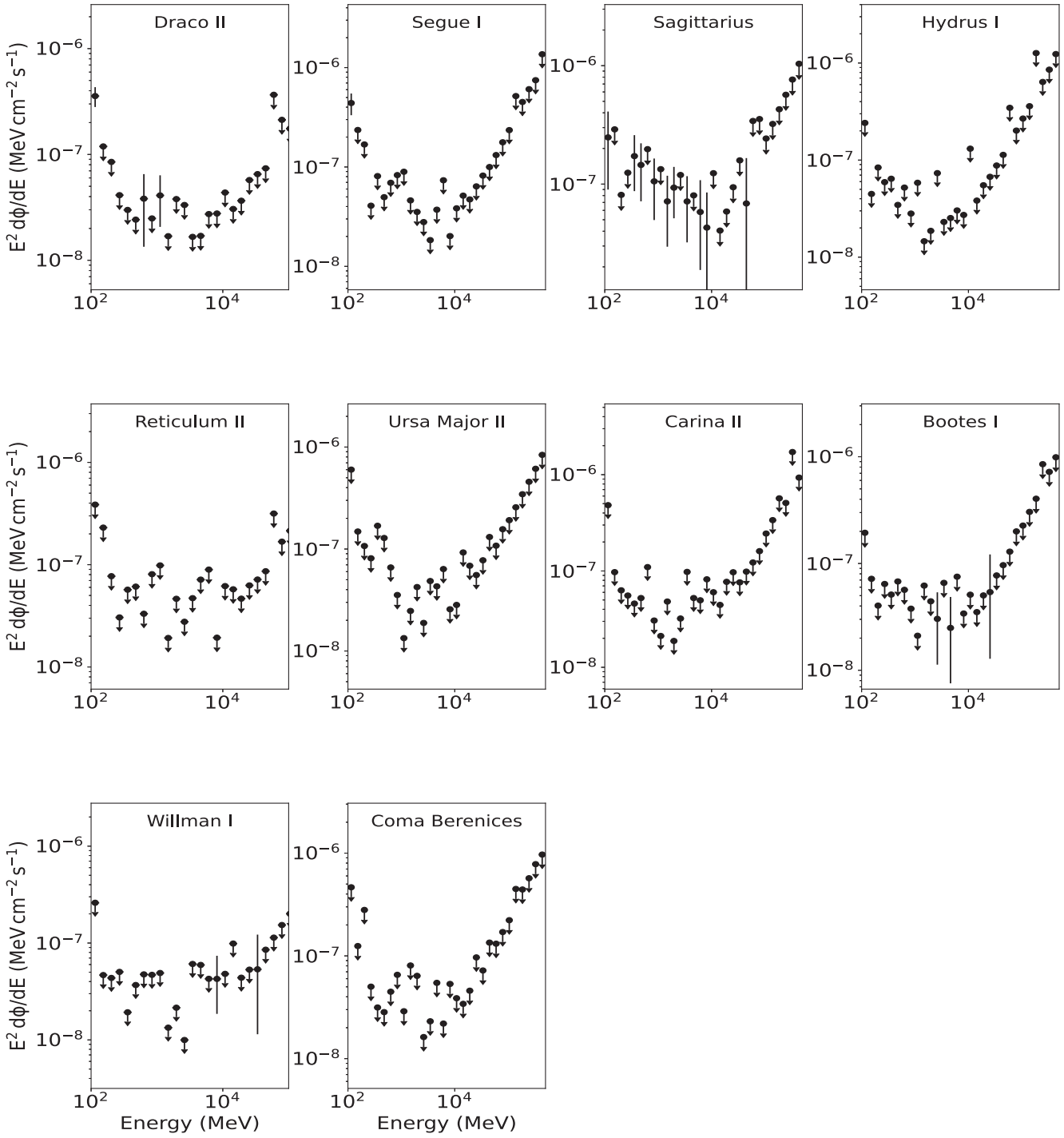

FIG. 1. Bin-by-bin flux upper limits at 95% CL observed by *Fermi*-LAT for our selected dSphs.

dSphs population, despite significantly smaller star counts. The stellar density can be modeled using a Plummer profile:

$$\rho_*(r) = \frac{3M_{*,\mathrm{tot}}}{4\pi R_*^3}\left(1+\frac{r^2}{R_*^2}\right)^{-5/2}, \tag{1}$$

where $M_{*,\mathrm{tot}}$ [55] is the stellar mass, expected to be $\sim N_{\mathrm{tot}} \times M_\odot$ and R_* is the stellar radius of each star related to the half-light radius (R_h) as $R_* = \sqrt{2^{2/3}-1}R_h$. N_{tot} represents the total expected number of stars in each dSph, determined by the stellar density profile of dwarf spheroidal galaxies. For the Plummer profile mentioned in Eq. (1), we adopt values from recent studies [55,61], where the number of member stars was derived by fitting the Plummer density profile to observational data. Alternatively, the star counts can be approximated using the luminosities of each dSph, as utilized

in [62]. We verify that both methods yield consistent results, with no significant impact on our conclusions. The maximum capture rate of DM particles by the stars of the dSphs is given by [63–66]

$$C_{\max} = \pi R_*^2 n_\chi(r) v_0 \left(1 + \frac{3}{2}\frac{v_{\rm esc}^2}{v_d(r)^2}\right). \tag{2}$$

The number density of DM particles, $n_\chi(r)$, at a distance r from the Galactic Center is $n_\chi(r) = \rho_\chi(r)/m_\chi$, where m_χ is DM mass and $\rho_\chi(r)$ is DM density. The velocity dispersion of the DM halo $v_d(r)$ is related to the orbital velocity $v_c(r)$ at distance r by $v_d^2(r) = \frac{3}{2}v_c^2(r)$, with $v_c^2(r) = \frac{GM(r)}{r}$, where G denotes the universal gravitational constant and $M(r)$ the mass of dSph within a radius of r. The average speed in the DM rest frame v_0 is computed using the relation $v_0^2 = \frac{8}{3\pi}v_d^2(r)$ and for escape velocity we use $v_{\rm esc}^2 = \frac{2GM_{1/2}}{R_{1/2}}$, where $M_{1/2}$ is the expected mass of dSphs contained within half-light radius, $R_{1/2}$. For the case of dSphs we fix $r = R_{1/2}, M(r) = M_{1/2}$. It should be noted that $M_{1/2}$ approximately can be expressed in terms of velocity dispersion of dSphs, $\sigma_{\rm l.o.s}$, as $M_{1/2} = \frac{2.5}{G}\sigma_{\rm l.o.s}^2 R_{1/2}$ [67].

To model the distribution of DM, we select the widely recognized Navarro-Frenk-White (NFW) density profile [68,69]. The NFW profile is particularly suited for describing DM halos in galaxies and clusters, capturing their density structure on a large scale. The general form of the NFW profile is given by

$$\rho_\chi^{\rm NFW}(r) = \rho_s \frac{r_s}{r}\left(1 + \frac{r}{r_s}\right)^{-2}, \tag{3}$$

where ρ_s and r_s represent the characteristic density and scale radius, respectively. In the present analysis, we use the analytical formulas[7] for r_s and ρ_s taken from Refs. [67,75].

In our investigation, in addition to single scattering, we also incorporate multiple scattering of DM particles as for massive DM particles, the energy loss in one collision may not be enough for gravitational capture. The inclusion of multiple collisions modifies the total capture rate of Eq. (2) as a series given by

$$C_{\rm tot}(r) = \sum_{n=1}^{\infty} C_{\rm n}(r), \tag{4}$$

where $C_{\rm n}$ denotes the capture rate corresponding to the "n" number of collisions after which the DM velocity falls below the escape velocity and eventually gets captured by dSph. The approximate formula for $C_{\rm n}$ is adopted from Refs. [76,77] and is written as

$$C_{\rm n}(r) = \pi R_{1/2}^2 \mathcal{P}_n(\tau)\frac{\sqrt{6}n_\chi(r)}{3\sqrt{\pi}v_d(r)}\left[(2v_d(r)^2 + 3v_{\rm esc}^2) - (2v_d(r)^2 + 3v_{\rm n}^2)\exp\left(-\frac{3(v_{\rm n}^2 - v_{\rm esc}^2)}{2v_d(r)^2}\right)\right], \tag{5}$$

where $v_{\rm n} = v_{\rm esc}(1 - \frac{2m_\chi m_{\rm n}}{(m_\chi + m_{\rm n})^2})^{-{\rm n}/2}$, with m_χ and $m_{\rm n}$ denoting the DM mass and mass of the nucleon, respectively. The probability $[\mathcal{P}_{\rm n}(\tau)]$ of the DM particles with optical depth τ to collide exactly n times before they get captured by the dSph can be written as

$$\mathcal{P}_{\rm n}(\tau) = 2\int_0^1 \frac{ze^{-z\tau}(z\tau)^{\rm n}}{{\rm n}!}dz. \tag{6}$$

The optical depth τ is defined in terms of DM-nucleon scattering cross section ($\sigma_{\chi n}$) as $\tau = \frac{3\sigma_{\chi n}N_T}{2\pi R_*^2}$, where $N_T = \frac{M_{*,\rm tot}}{m_n}$ is the total number of nucleons in the target.

B. Gamma-ray spectrum from DM annihilation via LLLMs

The captured DM particles may undergo self-annihilation if their accumulation inside dSph is sufficient. At time t, the evolution of the total number of captured DM particles $N(t)$ can be expressed as

$$\frac{dN(t)}{dt} = C_{\rm C} - C_{\rm E}N(t) - C_{\rm ann}N^2(t), \tag{7}$$

where $C_{\rm C}$ is the total capture rate, which is redefined as $C_{\rm C} = \min[C_{\rm tot}, C_{\max}]$ to properly incorporate the perturbative estimation, especially relevant for multiple scattering, while $C_{\rm E}$ denotes the rate at which the captured DM evaporates by scattering. In Eq. (7), $C_{\rm ann} = \langle\sigma_{\rm ann}v\rangle/V_0$ represents the annihilation rate with $\langle\sigma_{\rm ann}v\rangle$ and V_0 being the velocity averaged annihilation cross section and volume over which annihilation occurs. We find that the evaporation mass ($m_{\rm evp}$) of a typical dSph is around ∼8 GeV [78] which is higher than the $m_{\rm evp}$ of Sun, i.e., $m_\chi \geq 4$ GeV [79,80]. It is important to note that in the present analysis, we only consider the DM mass $m_\chi \gtrapprox 10$ GeV and for such higher DM masses, we can safely disregard the contribution of DM evaporation effect due to scattering ($C_{\rm E}$) in our calculation. Assuming the initial condition as $N(0) = 0$ at $t = 0$, the general solution of Eq. (7) is given by

$$N(t) = C_{\rm C}t_{\rm eq}\tanh(t/t_{\rm eq}), \tag{8}$$

where $t_{\rm eq}$ is the time required to reach equilibrium between DM capture and annihilation and is defined as

[7]It is worthwhile to mention here that though for the NFW parameters, namely, ρ_s and r_s, we use the above-mentioned expressions, we have also calculated the gamma-ray flux adopting the ρ_s and r_s values directly from the various Refs. [70–74] and compared with those obtained from the analytical expressions and we find no significant changes in the main results.

$$t_{\rm eq} = \frac{1}{\sqrt{C_{\rm C} C_{\rm ann}}}. \tag{9}$$

The dSphs are primarily composed of old, low-mass stellar populations. The majority of stars in dSphs are ancient, typically over 10^9 years old, having formed early in the universe's history. These stars are metal poor because star formation in dSphs ceased relatively early, limiting the enrichment of heavy elements. The equilibrium timescale, $t_{\rm eq}$, between DM annihilation and capture rate depends on the core density ($\rho_{\star,c}$) and core temperature ($T_{\star,c}$) of stars inside dSphs where annihilation takes place. In the case of dSph stars, accurately estimating these stellar properties is particularly challenging due to the limited availability of high-resolution photometric and spectroscopic studies. Consequently, it remains uncertain whether these systems have reached equilibrium. However, adopting a conservative approach, we assume equilibrium is achieved. Under this assumption, the total annihilation rate ($\Gamma_{\rm ann}$) of DM particles can be expressed as

$$\Gamma_{\rm ann} = \frac{C_{\rm ann} N^2}{2} \to \frac{C_{\rm C}}{2}, \tag{10}$$

where a factor of 2 indicates that, in each self-annihilation process, two DM particles participate. After computing the total annihilation rate, we can express the expected flux ($E^2 \frac{d\Phi}{dE_{\rm exp}}$) from DM annihilation for LLL mediators and later compare that with the observed differential flux of gamma rays at the *Fermi*-LAT detector by the following equations:

$$E^2 \frac{d\Phi}{dE_{\rm exp}} = \frac{\Gamma_{\rm ann}}{4\pi d^2} \times E^2 \frac{dN_\gamma}{dE}, \tag{11}$$

$$E^2 \frac{d\Phi}{dE_{\rm exp}} = E^2 \frac{d\Phi_\gamma}{dE}_{Fermi\text{-LAT}}, \tag{12}$$

where $\frac{dN_\gamma}{dE}$ is the gamma-ray spectrum from dSph and d denotes the heliocentric distance of dSph. In this work, we consider a model in which the spectrum dN_γ/dE originates from the decay of the mediators ($\chi\chi \to \phi\phi; \phi \to \gamma\gamma$) unlike the case where DM directly annihilates to gamma rays ($\chi\chi \to \gamma\gamma$). The two-step process has an advantage over the annihilation of DM particles directly to SM states as shown in Ref. [25]. In scenarios where DM directly annihilates into SM particles within astrophysical objects, the resulting flux of SM particles may be reduced due to further trapping within the object. However, if DM instead annihilates into SM particles through LLLMs (ϕ) that can escape the dSphs, the observable flux could be enhanced, increasing the potential for detection. Additionally, in this latter scenario, four photons are produced per annihilation, further boosting the gamma-ray flux compared to direct annihilation. Note that following Refs. [50,51], we also here ignore any possible interactions of the mediator and SM particles inside the dSphs and assume all the mediators decay outside the dSph yielding detectable gamma-ray flux. This two-step mechanism also assumes that the decay length of the mediator $L_\phi = \frac{m_\chi}{m_\phi \Gamma}$, with Γ being the decay width, is much larger than the half-light radius of dSph $R_{1/2}$. This automatically implies that the mediator should be "light," i.e., $m_\chi \gg m_\phi$ and "long-lived," i.e., the decay width should be very small or the mediator's lifetime (τ_ϕ) should be considerably long. This is indeed the case for the secluded DM models [24,25,45]. One can get an estimate of m_ϕ and τ_ϕ by using the fact that ϕ should decay outside the dSphs, i.e.,

$$L_\phi = \gamma_\phi c \tau_\phi \gg R_{1/2}, \tag{13}$$

where $\gamma_\phi = m_\chi/m_\phi$ is the boost factor and c denotes the speed of light in vacuum. Considering a half-light radius $R_{1/2} = 100$ pc and for DM mass in GeV-TeV scale, the typical values of the mediator lifetime and mass are $\tau_\phi \approx 10^{10}$ s and $m_\phi \ll \mathcal{O}(1)$ MeV (using $m_\chi/m_\phi \gg 10^{10}/\tau_\phi$). Mediators with such long lifetimes, particularly for indirect detection of DM, have been discussed in previous works; for instance, the positron excess has been explained using LLLMs in Refs. [44,46]. The authors in Ref. [81] have studied DM searches from dSphs from the decay of such LLLMs. From the cosmological point of view, such long-lived mediators are possible if their abundance is small enough during the early Universe. Several mechanisms to accommodate such scenarios are explored in Refs. [44,46,82]. Here, we mainly focus on the observations of DM annihilation via such LLLMs. Since, in the present work, we are considering DM mass $m_\chi \geq 10$ GeV, so for $m_\phi < \mathcal{O}(1)$ MeV the condition $m_\chi \gg m_\phi$ is satisfied all of the time.

With the assumptions mentioned above, the gamma-ray spectrum originating from the DM annihilation from dSphs through an LLLM is then given by a box-shaped spectrum described in [83] and can be written as

$$\frac{dN_\gamma}{dE} = \frac{4}{\Delta E} \Theta(E - E_-) \Theta(E_+ - E), \tag{14}$$

where Θ denotes the usual Heaviside function while the upper and lower limits of gamma-ray energy are written as $E_\pm = \frac{1}{2}(m_\chi \pm \sqrt{m_\chi^2 - m_\phi^2})$ which are also referred to the right (+ sign) and left (− sign) edges of the box. The width of the box is defined as $\Delta E = E_+ - E_- = \sqrt{m_\chi^2 - m_\phi^2}$, while the center is given by $E_0 = (E_+ + E_-)/2 = m_\chi/2$.

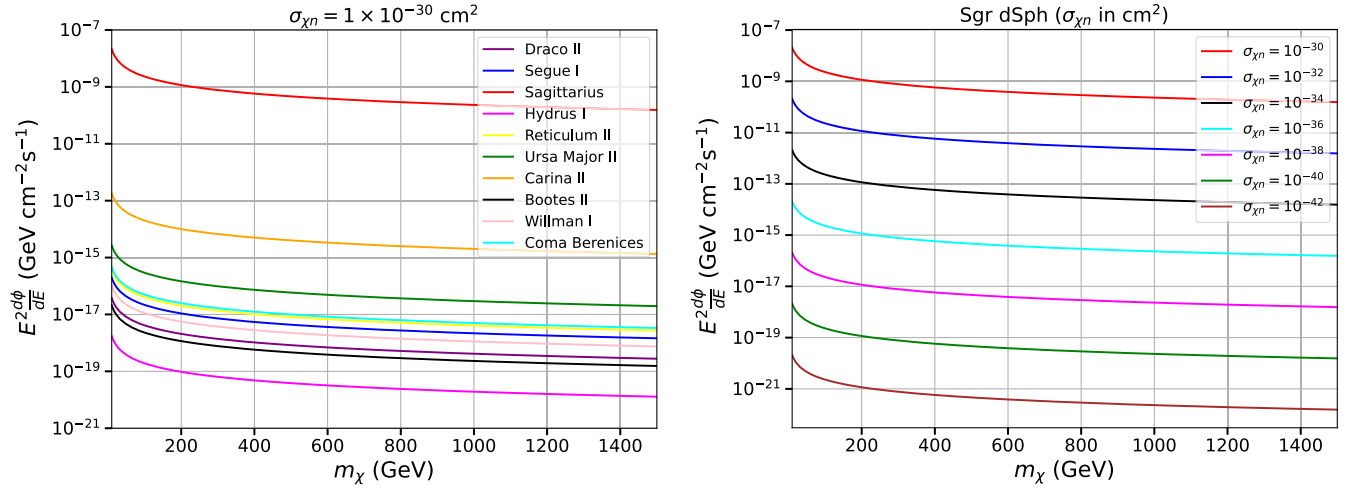

FIG. 2. Differential gamma-ray flux as a function of DM mass (m_χ) for ten different dSphs. The left (right) plot corresponds to a fixed (different) value of DM-nucleon scattering cross section ($\sigma_{\chi n}$).

V. EXPECTED FLUX FROM DM ANNIHILATING TO LLLMS FROM DSPHS

In this section, we study the expected flux from our targets following Eq. (11) for $m_\chi \gg m_\phi$. Figure 2 illustrates the variation of gamma-ray differential flux from DM annihilation as a function of DM mass for our selected dSphs. In Table II, we mention the values (and their associated uncertainties) of $R_{1/2}$, $M_{1/2}$, r_s, and ρ_s for all of our targets, which are crucial to derive the flux limits presented in Fig. 2. Here we would like to note that, throughout this paper, we adopt the central values of the parameter sets (see Tables I and II) to derive limits from the selected dSphs and in Sec. VII, we discuss how the uncertainty on parameter space can propagate through our obtained limits. The range of DM mass is taken from 10 to 1500 GeV, and a typical value of the DM nucleon scattering cross section, $\sigma_{\chi n} = 1 \times 10^{-30}$ cm^2, is adopted. It should be mentioned that, as long as the condition $m_\chi \gg m_\phi$ holds, the DM-induced gamma-ray flux limits are more or less independent of the mediator mass m_ϕ. With increasing mediator mass, the width of the spectrum changes, and the flux is shifted towards higher DM masses.

From the left panel of Fig. 2, we observe that for the Sagittarius (Sgr) dSph, the expected gamma-ray flux is stronger compared to other chosen dSphs. This is because Sgr has significantly higher $M_{*,\mathrm{tot}}$ and R_*, leading to increased DM accumulation and, consequently, a higher DM annihilation rate compared to other dSphs such as Draco II and Segue I. Therefore, we expect the Sgr bounds on DM parameter space to be stronger than other dSphs. The right plot of Fig. 2 displays how the gamma-ray flux from Sgr dSph varies with different values of $\sigma_{\chi n}$. We show the expected behavior of flux, i.e., the flux decreases with the DM-nucleon scattering cross section. This occurs because higher scattering cross sections result in more efficient capture of DM by the stellar component, reducing

TABLE II. Sample of dSphs used in this study with the median value of their associated NFW density profile parameters. column I: $M_{1/2}$ in unit $M_\odot$ [57,58]; column II: $R_{1/2}$ in (pc) [57,58]; column III: ρ_s in unit GeV/cm^3; and column IV: r_s in unit kpc. The values of ρ_s and r_s are computed following the expressions given in [67,75].

Source	$M_{1/2}$ ($M_\odot$)	$R_{1/2}$ (pc)	ρ_s (GeV/cm^3)	r_s (kpc)
Draco II	$< 5.34 \times 10^5$	$16.01^{+3.60}_{-3.51}$	$< 44.13^{+30.19}_{-13.57}$	$0.08^{+0.02}_{-0.02}$
Segue I	$2.45^{+2.06}_{-1.39} \times 10^5$	$19.51^{+3.38}_{-3.13}$	$11.69^{+20.45}_{-7.41}$	$0.09^{+0.01}_{-0.01}$
Sagittarius	$1.88^{+0.30}_{-0.26} \times 10^8$	$1565.80^{+133.09}_{-126.16}$	$0.02^{+0.01}_{-0.01}$	$7.83^{+0.66}_{-0.63}$
Hydrus I	$3.50^{+1.43}_{-1.13} \times 10^5$	$52.42^{+5.33}_{-5.55}$	$0.86^{+0.67}_{-0.36}$	$0.26^{+0.03}_{-0.03}$
Reticulum II	$4.30^{+2.46}_{-1.85} \times 10^5$	$36.46^{+5.25}_{-5.61}$	$3.17^{+4.18}_{-1.57}$	$0.18^{+0.03}_{-0.03}$
Ursa Major II	$3.83^{+1.82}_{-1.44} \times 10^6$	$92.06^{+7.40}_{-7.03}$	$1.72^{+1.24}_{-0.79}$	$0.46^{+0.03}_{-0.03}$
Carina II	$8.12^{+5.79}_{-4.06} \times 10^5$	$76.51^{+7.69}_{-7.72}$	$0.64^{+0.82}_{-0.33}$	$0.38^{+0.04}_{-0.04}$
Bootes II	$2.52^{+3.19}_{-1.84} \times 10^5$	$32.99^{+5.01}_{-5.03}$	$2.51^{+6.05}_{-1.85}$	$0.16^{+0.02}_{-0.02}$
Willman I	$2.90^{+1.59}_{-1.13} \times 10^5$	$19.97^{+4.51}_{-4.12}$	$13.04^{+17.78}_{-7.28}$	$0.09^{+0.02}_{-0.02}$
Coma Berenices	$1.07^{+4.22}_{-3.46} \times 10^6$	$54.94^{+4.12}_{-4.19}$	$2.278^{+1.42}_{-0.93}$	$0.27^{+0.02}_{-0.02}$

the available annihilation rate and, hence, the resulting gamma-ray flux.

VI. BOUNDS ON THE DM SCATTERING CROSS SECTION WITH DSPHS STARS FROM *FERMI*-LAT DATA

The objective of this paper is to derive the constraints on DM parameter space using *Fermi*-LAT flux upper limits from the direction of our selected dSphs. In Sec. III we present the bin-by-bin differential flux upper limits (Fig. 1). We perform the binned likelihood analysis by defining the total likelihood function $\mathcal{L}_{i,j}$ for ith dSph at the jth energy bin which can be written as

$$\mathcal{L}_{i,j} = e^{-N_{\rm exp}} \prod_j \frac{\lambda^{n_j}{}_{i,j}}{n_j!}, \tag{15}$$

where n_j denotes the measured number of counts while $N_{\rm exp}$ is the total number of expected counts from the source model, including signal and background predictions, and for each dSph the expected count in jth bin is labeled as $\lambda_{i,j}$. Now for a given DM mass, we calculate the expected flux from dSphs using Eqs. (11) and (14) for box-shaped spectrum and then compare this flux with the *Fermi*-LAT upper limits shown in Fig. 1 following Eq. (12). We obtain the bounds on DM annihilation rate $\Gamma_{\rm ann}$ which eventually get translated into the DM parameter space $(m_\chi - \sigma_{\chi n})$ in Fig. 3 corresponding to R_* and $M_{*,\rm tot}$ values of each dSphs (Table I).

We also perform the stacked analysis using the joint likelihood method ($\mathcal{L}_{\rm joint} = \prod_i \mathcal{L}_i$). In Fig. 3, the stacked constraints are shown in a dashed red color curve. As expected from Fig. 2, in Fig. 3 we similarly observe that the strongest bound on the DM-nucleon scattering cross section comes from Sgr dSph.

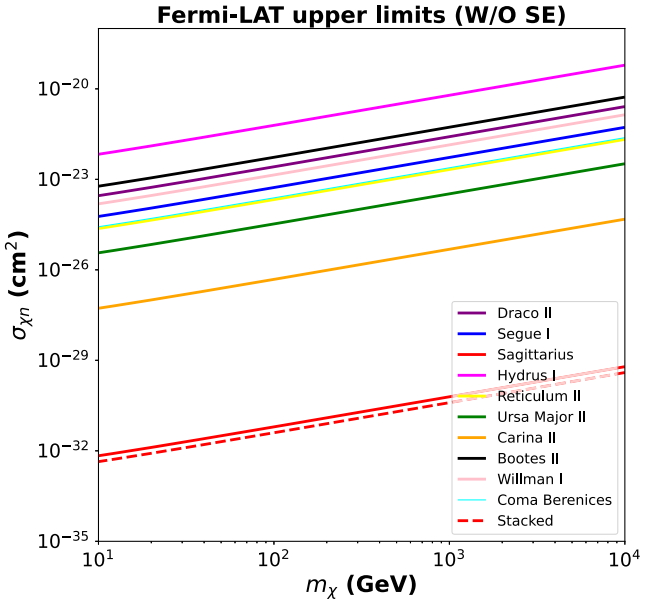

FIG. 3. Upper limits on DM mass versus DM-nucleon scattering cross section from individual dSphs and from combined all dSphs (stacked) using the *Fermi*-LAT data.

We find that the scattering cross section of DM with nucleon can be probed as stringent as $\sim 10^{-33}$ cm^2 from the stacked limits. In our study, we assume the equilibrium hypothesis between the DM capture rate inside the dSphs stellar population and the annihilation rate to obtain the most stringent limits in a conservative approach. Our relatively weak constraints on the scattering cross section compared to other astrophysical sources [84] stem from the shallower gravitational potential wells of dSphs. This results in lower DM densities within the stellar bodies, reducing the capture rate and the subsequent annihilation signal. Nonetheless, these galaxies remain invaluable targets due to their low background contamination and the unique insights they provide into DM interactions.

To improve the bounds on the DM-nucleon scattering cross section, future telescopes with higher sensitivity to gamma rays and broader energy coverage, such as the Cherenkov Telescope Array (CTA) [85], will play a pivotal role. These instruments will enable deeper and more precise observations of dSphs, providing critical data to refine our constraints. Additionally, the application of the Sommerfeld enhancement (SE) [86], which accounts for the velocity-dependent amplification of the DM annihilation rate at low velocities, can offer a promising avenue for tightening our current bounds. This effect is particularly relevant for dSphs, where DM particles are expected to have low velocity dispersions, making them an ideal environment for probing this phenomenon. Following this motivation, in the later section, we examine how the SE can impact and improve our current bounds obtained from this model-independent approach.

VII. EFFECT OF ASTROPHYSICAL UNCERTAINTIES

In this section, we assess the impact of observational uncertainties in key physical parameters on the predicted gamma-ray flux and the resulting constraints on the DM-nucleon scattering cross section. This is particularly relevant, as such uncertainties propagate into the inferred dark matter density profiles. We consider the Sgr dSph as a representative case, given that it yields the most stringent bounds on $\sigma_{\chi n}$ among the ten dSphs studied. Although similar analyses can be performed for the remaining targets, Sgr dominates the stacked constraint, with the next most constraining system, Carina II, producing limits that are approximately $\mathcal{O}(4\text{–}5)$ times weaker (see Fig. 3). We therefore restrict our analysis to Sgr to estimate the potential impact of parameter uncertainties on the final results. This issue is revisited in the discussion section.

From Eqs. (3) and (11), we understand that the gamma-ray fluxes from DM annihilation are subject to uncertainties

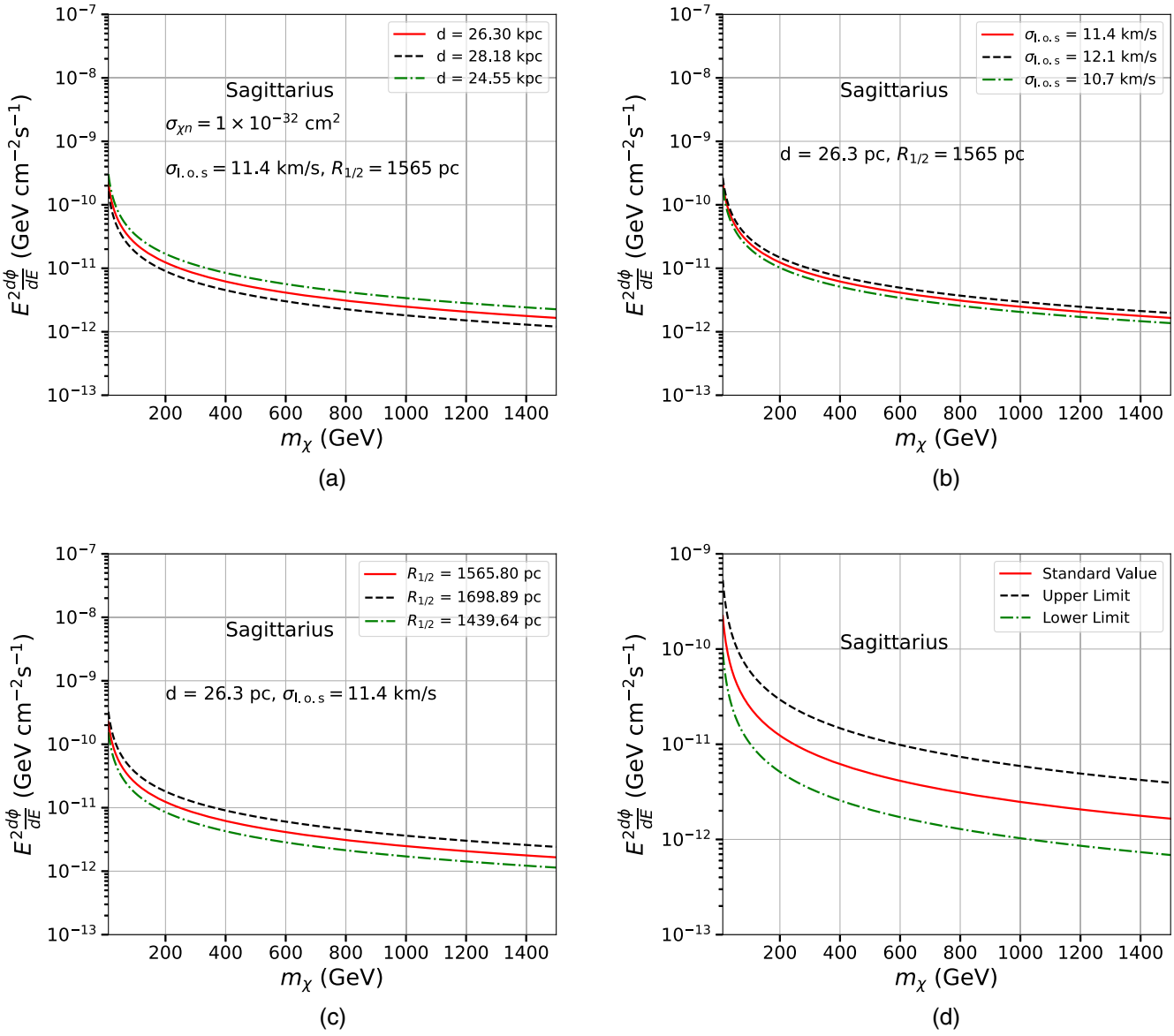

FIG. 4. Effect of individual and combined astrophysical uncertainties on DM annihilation fluxes from Sgr dSph. The uncertainty on the fluxes can originate from the observational uncertainties on the measurement of dSph parameters (a) d, (b) $\sigma_{\rm l.o.s}$, and (c) $R_{1/2}$. The variations on these dSph parameter values will affect the r_s and ρ_s values used in the dSph DM profile [Eq. (3)].

on account of the errors in determining the astrophysical parameters d (heliocentric distance), ρ_s (characteristic density), and r_s (scale radius). The values of ρ_s and r_s are computed from analytical expressions given in Refs. [67,75] which in turn depend upon $R_{1/2}$ (half-light radius) and $\sigma_{\rm l.o.s}$ (velocity dispersion). Thus, the main source of uncertainties in the flux comes from ambiguity in the determination of d, $R_{1/2}$, and $\sigma_{\rm l.o.s}$. Using the central values for these dSph parameters, the bounds on $\sigma_{\chi n}$ are displayed in Fig. 3. Here, we first study the effect of individual uncertainty by varying one parameter at a time. To this end, in Fig. 4, we present the possible uncertainties in the DM-induced gamma-ray fluxes as a consequence of ambiguities in d [Fig. 4(a)], $\sigma_{\rm l.o.s}$ [Fig. 4(b)], $R_{1/2}$ [Fig. 4(c)], and combining all three contributions [Fig. 4(d)]. We fix $\sigma_{\chi n} = 1 \times 10^{-32}$ cm^2 for all of the plots in Fig. 4 and the relevant parameters of Sgr dSph are varied within their 1σ uncertainties mentioned in Tables I and II. In all plots of Fig. 4, the standard gamma-ray fluxes (shown in red color curves) are computed using the central values of the dSph parameters. For simplicity and in the absence of adequate information, we assume no correlations among these three parameters. We notice from Fig. 4(b) that the error in the dispersion velocity $\sigma_{\rm l.o.s}$ has the least effect on the gamma-ray fluxes, while the actual uncertainty band, which is a combination of all three contributions and presented in Fig. 4(d), shows 5–8 times uncertainty in the fluxes from the central values (red color curve). It should also be noted

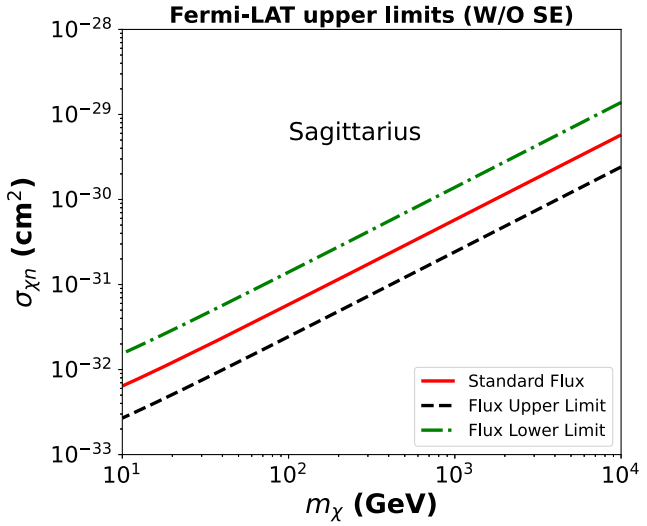

FIG. 5. Effect of astrophysical uncertainties on the DM-nucleon scattering cross-section bounds from Sgr dSph. The black (green) limits correspond to the case where upper (lower) flux values are used, considering the uncertainties (1σ) in dSph parameters.

that, due to the large relative error in $R_{1/2}$ measurement, this parameter contributes more to the flux uncertainty and, hence, should be measured more precisely. Finally, we propagate the uncertainty in the DM-induced gamma-ray fluxes into the DM-nucleon scattering cross section $\sigma_{\chi n}$ and the result is displayed in Fig. 5 in the $\sigma_{\chi n} - m_\chi$ plane for Sgr dSph. The bounds shown in red color correspond to the case where central values of dSph parameters are used, while the band between green and black color represents the maximum possible uncertainty in the constraints for Sgr dSph. From Fig. 5 we observe that the maximum error in the bounds on $\sigma_{\chi n}$ can be of $\mathcal{O}(1)$.

VIII. EFFECT OF SOMMERFELD ENHANCEMENT ON SCATTERING CROSS-SECTION UPPER LIMITS

In this section, we study a scenario where DM annihilation occurs through LLLMs, incorporating the Sommerfeld enhancement (SE), first introduced by Arnold Sommerfeld in 1931 [86], into the DM annihilation cross section. This effect refers to the fact that, in the presence of long-range attractive potential, the annihilation cross section of non-relativistic DM particles is significantly enhanced, leading to a larger observational signal. The Sommerfeld effect is more pronounced at low relative velocities (Sommerfeld factor $\propto 1/\text{velocity}$) and dSphs are considered some of the best targets to observe such phenomena because the relative velocities of DM particles in dSphs tend to be much lower than other astrophysical objects such as galaxy clusters or Milky Way [22,87].

It should be noted that the effects of the SE depend upon the nature of the force carrier [45,88] as the annihilation cross section and, hence, the Sommerfeld factor would be different for different force carriers. In Refs. [30,49,89,90], for instance, the mediator is a vector gauge boson (dark photon model) which gives neutrino as DM signal. However, the decay of a vector boson directly into two gamma-ray photons is forbidden [30], i.e., if ϕ is a dark photon, $\phi \to \gamma\gamma$ is prohibited. We, therefore, adopt a very simple model in order to get gamma-ray flux from the decay of the mediator ϕ along with the inclusion of the SE.

For the DM model considered here, we assume that the DM particles experience a long-range force mediated by an LLLM, ϕ, before they undergo self-annihilation into the same mediator ϕ which later decays to produce a detectable gamma-ray signal. So, in this very simplified model, we have the same mediator ϕ that induces the Sommerfeld effect as well as provides a box-shaped spectrum due to DM annihilation via LLLM. Under this assumption, the SE-induced annihilation cross-section rate $[\langle\sigma_{\rm ann}v\rangle_S]$ can be expressed as the product of the Sommerfeld factor and the Born-approximated annihilation cross section $[\langle\sigma_{\rm ann}v\rangle_{\rm Born}]$, as shown below [20]:

$$\langle\sigma_{\rm ann}v\rangle_S = \langle\sigma_{\rm ann}v\rangle_{\rm Born}\langle S_{\rm swave}\rangle, \tag{16}$$

where $\langle S_{\rm swave}\rangle$ denotes the thermally averaged SE factor for s wave and we consider ϕ as a scalar particle that may eventually decay into two gamma photons. Another important assumption we make to maximize the gamma-ray flux is that the DM particle is also a scalar [91,92].[8] In that case, the thermally averaged annihilation cross section at the tree level (for scalar DM interacting with a scalar mediator) is given by [95]

$$\langle\sigma_{\rm ann}v\rangle_{\rm Born} = \frac{\pi\alpha_\chi^2\varepsilon_\phi^4}{4m_\chi^2}\frac{\sqrt{1-\varepsilon_\phi^2}}{(1-\varepsilon_\phi^2/2)^2}, \tag{17}$$

where $\varepsilon_\phi = m_\phi/m_\chi$ and $\alpha_\chi = g_\chi^2/4\pi$ represent the dark fine structure constant with g_χ being the gauge coupling of the long-range force mediated by ϕ. The enhancement factor for s-wave thermally averaged annihilation can be expressed as [96,97]

$$\langle S_{\rm swave}\rangle = \int \frac{S_{\rm swave}(e^{-v^2/2v_0^2})}{(2\pi v_0^2)^{3/2}} d^3v, \tag{18}$$

where the DM velocity inside the object is $v_0 = \sqrt{2T_{\star,c}/m_\chi}$. In our dSphs analysis, we use $T_{\star,c} \sim 30000K \sim 2.59\times10^{-9}$ GeV [98]. The s-wave SE factor

[8]Although we have focused on the scalar DM case for SE, a fermionic scenario can also be considered; see, e.g., [54,93,94]. However, the main issue is that, for a fermion, the $\chi\chi \to \phi\phi$ annihilation process suffers from p-wave suppression reducing the gamma-ray signal from dSphs. We plan to consider such cases in future work.

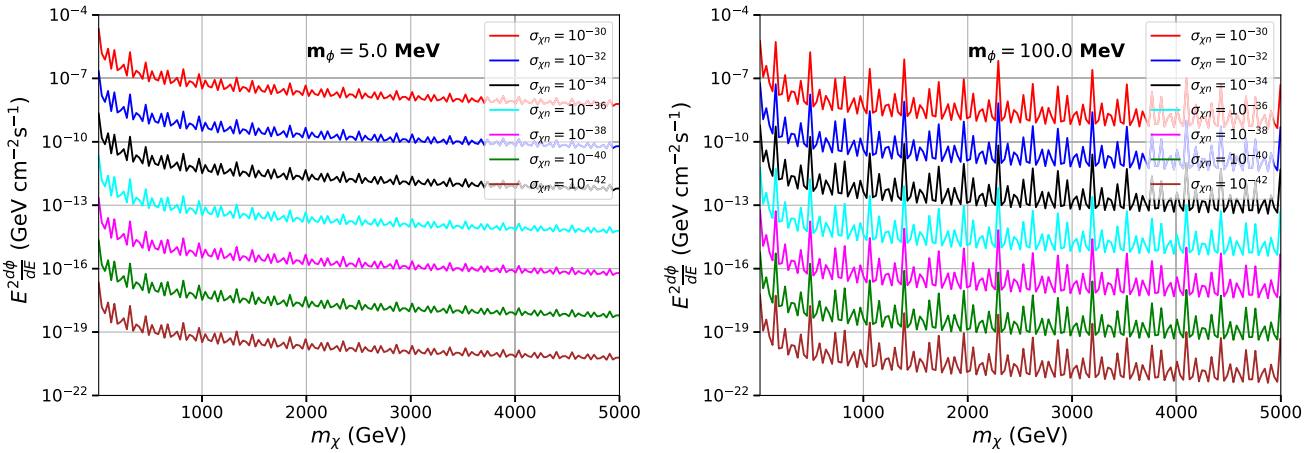

FIG. 6. Effect of SE on DM annihilation flux from Sgr dSph. The left (right) plot corresponds to the mediator mass $m_\phi = 5.0(100.0)$ MeV. The rapid oscillation in the flux is a distinctive feature of the Sommerfeld effect owing to the formation of bound states near the threshold in the presence of attractive potential [22,100–102].

($S_{\rm swave}$) can be derived analytically by approximating the Yukawa-type long-range interaction for nonzero mediator mass to the Hulthén potential and is given by [88,96,97,99]

$$S_{\rm swave} = \frac{\pi}{\beta}\frac{\sinh 2\pi\beta\zeta}{\cosh 2\pi\beta\zeta - \cos(2\pi\sqrt{\zeta - \beta^2\zeta^2})}, \quad (19)$$

where $\beta = v/(2\alpha_\chi)$ and $\zeta = 6\alpha_\chi m_\chi/(\pi^2 m_\phi)$.

We compute the total annihilation rate, i.e., $\Gamma_{\rm ann}$, and thereby the annihilation flux of gamma rays in the presence of SE by employing equations from (16) to (19) and Eq. (10). Next, we determine the value of α_χ by fixing the annihilation rate at freeze-out as $\langle\sigma_{\rm ann}v\rangle = 2.2 \times 10^{-26}$ cm^3/s [79] to satisfy the DM thermal relic density $\Omega_\chi h^2 = 0.12$ which implies

$$\alpha_\chi = \left(\frac{0.097}{\epsilon_\phi^2}\right)\left(\frac{m_\chi}{\rm TeV}\right). \quad (20)$$

In Fig. 6 we demonstrate the Sommerfeld enhanced gamma-ray flux for Sgr dSph as a function of DM mass for different values of scattering cross section, $\sigma_{\chi n}$. The left (right) plot corresponds to the mediator mass $m_\phi = 5.0(100.0)$ MeV. The wiggles in Fig. 6 represent the usual nature of the SE. We observe that the flux is getting significantly enhanced due to the Sommerfeld effect (compare Figs. 2 and 6). Moreover, we also notice a slight dependence of gamma-ray flux on the mediator mass m_ϕ. We then compute the bounds on DM scattering cross section as a function of DM mass following the same approach mentioned in Sec. VI using *Fermi*-LAT upper limits derived in Fig. 1. The results are furnished in Fig. 7 for both individual dSph and stacked analyses.

From Fig. 7, it is evident that the inclusion of the SE significantly strengthens the constraints, improving them by nearly 3 to 4 orders of magnitude compared to the case without SE (Fig. 3). The current limits reach $\sim 10^{-36}$ cm^2 for DM masses around 100 GeV. This happens due to the presence of long-range attractive interaction of DM particles mediated by LLLMs; the equilibrium timescale reduces significantly, increasing the DM annihilation flux to its maximum value. It is to be noted that with the increase of the mediator mass from m_ϕ the bounds become better to some extent. Similar observations have been shown in Fig. 6 of Ref. [49]. We also notice the rapid oscillations in Fig. 7 which is a well-known feature of the SE due to the formation of bound (or resonancelike) states.

In Fig. 8, we compare our results, both with SE and without SE, to the limits reported by various direct detection [103–105] and astrophysical observations [47,50,84,106]. Our limits are far above those reported by underground direct detection experiments by CDMS II [103], PICO 60 [104], and DEAP 3600 [105]. Moreover, we also plot the limits from other astrophysical studies performed on Galactic Center (GC) stars [84], GC population of brown dwarfs (BDs) [50], white dwarfs (WDs) [106], and Jupiter [47]. We notice that for DM mass around 10–20 GeV, our limits are comparable to those obtained from BDs, and for higher DM masses ($> \sim$500 GeV) stacked dSphs bounds are stronger than Jupiter. Although the resulting bounds on DM-nucleon interactions derived from dSphs are weaker compared to those obtained from direct detection experiments or more massive compact objects like BDs and WDs, they offer the advantage of being cleaner, and relatively free from significant astrophysical backgrounds. Furthermore, investigating the DM capture rate within the stellar populations of dSphs complements traditional indirect DM searches in these

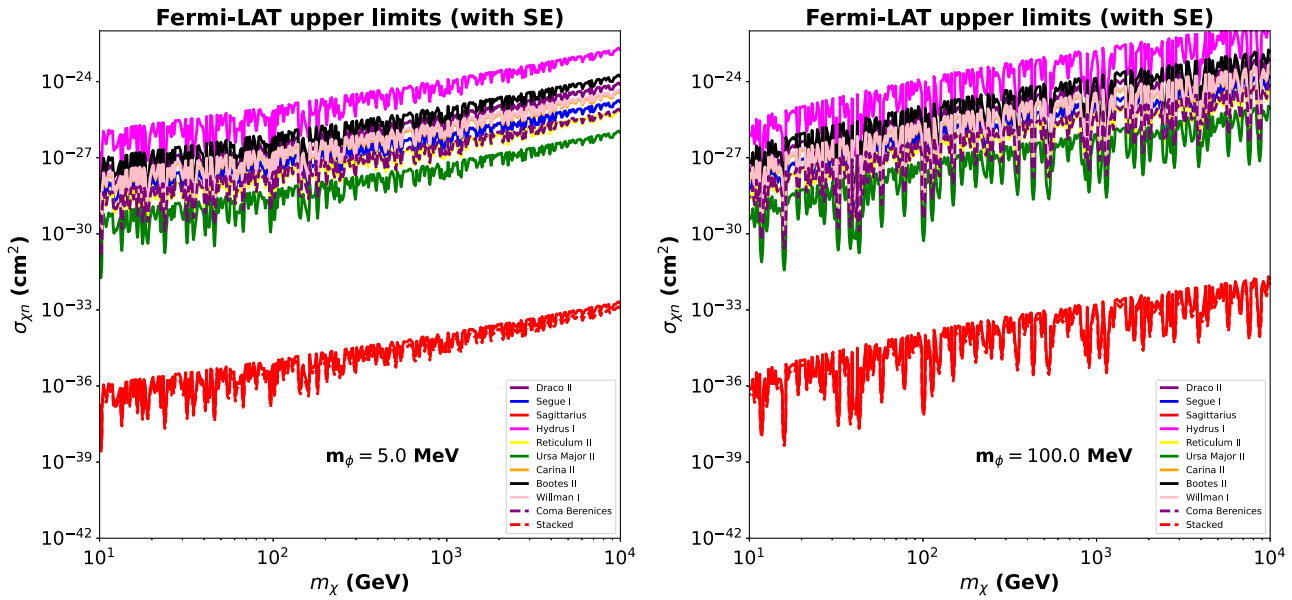

FIG. 7. Upper limits on DM-nucleon scattering cross section as a function of DM mass including the SE using the *Fermi*-LAT data. The left (right) plot corresponds to the mediator mass $m_\phi = 5.0(100.0)$ MeV.

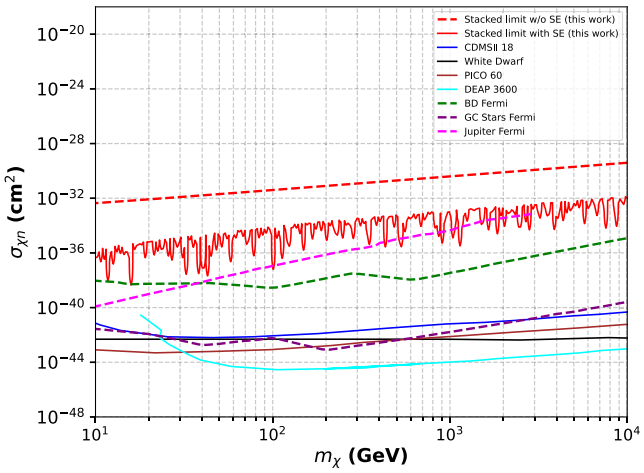

FIG. 8. Comparison between the bounds obtained from dSphs in this work with those already available in the literature. We also display the direct detection constraints on spin-independent DM-nucleon cross sections from different experiments such as CDMS II [103], PICO 60 [104], and DEAP 3600 [105], and the indirect detection bounds from other astrophysical objects are adapted from Refs. [47,50,84,106].

galaxies [7,107], thereby enhancing the comprehensive exploration of DM properties.

IX. CONCLUSION AND DISCUSSION

This paper investigates the DM signal from nearby dSphs (< 50 kpc distance), considering a phenomenological framework in which DM particles first capture within the stars inside dSph and subsequently annihilate into LLL mediators. The mediator will later decay into gamma rays that can be detected by gamma-ray telescopes such as *Fermi*-LAT. For this, we have analyzed nearly 16 years of data from *Fermi*-LAT to look for the gamma-ray emission from the selected dSphs and present the observed limits in Fig. 1. In the absence of any excess signal, we estimate the 95% CL conservative upper limits on DM-nucleon scattering cross section ($\sigma_{\chi n}$) as a function of DM mass (m_χ).

We find that Sgr dSph provides the best limits among all other dSphs considered in this work, and the stacked limits can be as low as $\sim 10^{-33}$ cm^2. Since our goal is to estimate the maximum possible upper limits expected from dSphs while exploring the two-step (cascade) process of DM annihilation into gamma photons, we assume that equilibrium is achieved between DM capture and annihilation. This maximizes the rate at which captured DM annihilates into mediators, making our bounds conservative. However, the equilibrium timescale is somewhat larger than the actual age of the dSphs, and the bounds might get weakened if the above-mentioned assumption is relaxed.

In the later part of this work, a particular model has been considered where both DM and the mediator are scalar particles. This further allows us to explore an interesting phenomenon, SE, in which, owing to the presence of long-range attractive potential sourced by the scalar mediators, the DM annihilation cross section and, hence, the detection prospects of such DM candidates enhance significantly. This is particularly important when the DM dispersion velocity is low, as in the case of dSphs. We show the resonancelike features of the SE in the DM-induced gamma-ray flux in Fig. 6 that are also reported in [49]. We notice that the effect of the mediator mass, m_ϕ, on the gamma-ray flux is not very significant, and it changes only

by a factor of a few. We then derive the upper limits on DM-nucleon scattering cross section in the presence of SE following a similar approach as mentioned in Sec. VI. As expected, the limits are significantly improved for Sgr dSph (and also for the stacked limit) with the inclusion of the SE.

Our study also highlights the impact of observational uncertainties in key astrophysical parameters on the gamma-ray flux from DM annihilation in dSphs. Using Sgr as a representative case, we find that variations—especially in the half-light radius $R_{1/2}$—can lead to significant shifts in the derived limits on the DM-nucleon scattering cross section, with uncertainties reaching up to $\mathcal{O}(1)$. This underscores the need for more precise kinematic and structural measurements of dSphs to strengthen indirect DM searches. Although the uncertainty analysis was performed for the case without SE, similar conclusions are expected in its presence, as the SE factor $\langle S_{\rm swave} \rangle$ [see Eq. (18)] does not depend on the dSph parameters d, $R_{1/2}$, or $\sigma_{\rm l.o.s}$, and is thus largely free from astrophysical uncertainties. Therefore, we expect an average error of $\mathcal{O}(1)$ in the limits on $\sigma_{\chi n}$ for both SE and no SE cases.

Finally, the bounds on the DM-nucleon cross section derived in this work are compared to those available in other studies as illustrated in Fig. 8. The constraints shown in Fig. 8 remain much weaker than those reported by underground direct detection experiments. Even in the presence of SE, the sensitivity obtained in the present analysis is several orders of magnitude above the current best experimental limits (say at 100 GeV, $\sigma_{\chi n} < 10^{-46}$ cm^2 [108,109]). On comparison with the bounds from other celestial objects, we see that the stacked dSphs upper limits (in the presence of SE) are stronger than Jupiter [47] for the DM masses above ∼500 GeV and comparable to the BDs limits [50] for masses in the 10–20 GeV range. We also note that the direct detection bounds from various experiments represent the model-independent limits whereas the Sommerfeld enhanced constraints on $\sigma_{\chi n}$ derived in this work are model dependent. Other model-independent bounds on the DM parameter space come from the cosmic structure formation which mainly rely on DM-nucleon scattering and not on the details of the particle nature of DM. A few related works on the study of DM interactions from structures formation are; limits from Lyman-alpha forest observations [110], abundance of Milky Way satellite galaxies [111–113], and cosmic microwave background (CMB) measurements [114,115]. However, all of these bounds are more than 2 orders of magnitude weaker in the GeV-TeV mass range than the ones obtained in this work. Indeed the structure formation limits on $\sigma_{\chi n}$ are very significant for the light (sub-GeV) DM scenarios where direct detection experiments have limited sensitivity. In this regard, we want to highlight that, even though dSphs are weaker than other current studies to capture DM, they provide a relatively cleaner environment due to the lack of gas and minimal astrophysical backgrounds. These results contribute to a broader understanding of DM properties, offering constraints that avoid some of the systematic uncertainties inherent in direct detection experiments and complement existing astrophysical bounds. Together, these findings underline the value of multifaceted approaches to probing the elusive nature of DM and its interactions.

To the best of our knowledge, this study represents one of the first attempts to probe the stellar component of dSphs to investigate the DM capture rate. By adopting a dual approach of both model independent and model dependent (incorporating the SE effect), our analysis offers a comprehensive framework for constraining the DM nucleon scattering cross section. This novel perspective sheds light on the potential role of stellar bodies within dSphs as complementary probes of DM interactions, emphasizing their significance alongside other astrophysical sources.

Our study also points to a new and alternative avenue for exploring DM phenomena in dSphs, particularly by highlighting the importance of incorporating velocity-dependent effects, such as the SE, to refine existing bounds. Future telescopes with enhanced sensitivity, such as the CTA, and advancements in stellar modeling are expected to provide critical improvements in the accuracy of DM capture rate estimations. Furthermore, the framework established in this work underscores the value of low-velocity environments in DM studies, offering a fresh perspective on the interplay between stellar populations and DM annihilation. These insights pave the way for a more holistic understanding of DM behavior across diverse astrophysical settings.

ACKNOWLEDGMENTS

We thank Amit Dutta Banik for the important and detailed discussions on Sommerfeld enhancement and constructive suggestions on our work. We also thank Ranjan Laha, Anirban Das, and Satyanarayan Mukhopadhyay for the useful discussions. P. B. acknowledges support from the COFUND action of Horizon Europe's Marie Sklodowska-Curie Actions research program, Grant Agreement No. 101081355 (SMASH). A. G. further wishes to acknowledge the organizers of the "Trends in Astro-particle and Particle Physics (TAPP 2024)" at the Institute of Mathematical Sciences, Chennai, India, during 25th to 27th September 2024 and the "XXVI DAE-BRNS High Energy Physics (HEP) Symposium 2024" at Banaras Hindu University (BHU), Varanasi, India, during 19th to 23rd December 2024, for providing an opportunity to present the preliminary results from this work.

DATA AVAILABILITY

The data supporting this study's findings are available within the article.

[1] M. G. Walker, M. Mateo, E. W. Olszewski, J. Penarrubia, N. W. Evans, and G. Gilmore, A universal mass profile for dwarf spheroidal galaxies, Astrophys. J. **704**, 1274 (2009).

[2] E. L. Lokas, Dark matter distribution in dwarf spheroidal galaxies, Mon. Not. R. Astron. Soc. **333**, 697 (2002).

[3] G. Battaglia, A. Helmi, and M. Breddels, Internal kinematics and dynamical models of dwarf spheroidal galaxies around the Milky Way, New Astron. Rev. **57**, 52 (2013).

[4] M. Walker, *Dark Matter in the Galactic Dwarf Spheroidal Satellites* (Springer, Netherlands, 2013), pp. 1039–1089.

[5] L. E. Strigari, Dark matter in dwarf spheroidal galaxies and indirect detection: A review, Rep. Prog. Phys. **81**, 056901 (2018).

[6] I. Esteban, A. H. G. Peter, and S. Y. Kim, Milky Way satellite velocities reveal the dark matter power spectrum at small scales, Phys. Rev. D **110**, 123013 (2024).

[7] A. McDaniel, M. Ajello, C. M. Karwin, M. Di Mauro, A. Drlica-Wagner, and M. A. Sánchez-Conde, Legacy analysis of dark matter annihilation from the Milky Way dwarf spheroidal galaxies with 14 years of Fermi-LAT data, Phys. Rev. D **109**, 063024 (2024).

[8] A. A. Abdo *et al.* (Fermi-LAT Collaboration), Observations of Milky Way dwarf Spheroidal galaxies with the Fermi-LAT detector and constraints on dark matter models, Astrophys. J. **712**, 147 (2010).

[9] M. Ackermann *et al.* (Fermi-LAT Collaboration), Constraining dark matter models from a combined analysis of Milky Way satellites with the Fermi large area telescope, Phys. Rev. Lett. **107**, 241302 (2011).

[10] M. Ackermann *et al.* (Fermi-LAT Collaboration), Dark matter constraints from observations of 25 Milky Way satellite galaxies with the Fermi large area telescope, Phys. Rev. D **89**, 042001 (2014).

[11] M. Ackermann *et al.* (Fermi-LAT Collaboration), Searching for dark matter annihilation from Milky Way dwarf spheroidal galaxies with six years of Fermi large area telescope data, Phys. Rev. Lett. **115**, 231301 (2015).

[12] A. Drlica-Wagner *et al.* (Fermi-LAT and DES Collaborations), Search for gamma-ray emission from DES dwarf spheroidal galaxy candidates with Fermi-LAT data, Astrophys. J. Lett. **809**, L4 (2015).

[13] A. Albert *et al.* (Fermi-LAT and DES Collaboration), Searching for dark matter annihilation in recently discovered Milky Way satellites with Fermi-LAT, Astrophys. J. **834**, 110 (2017).

[14] M. Ackermann *et al.* (Fermi-LAT Collaboration), Search for dark matter satellites using the FERMI-LAT, Astrophys. J. **747**, 121 (2012).

[15] M. Ajello *et al.* (Fermi-LAT Collaboration), Fermi-LAT observations of high-energy γ-ray emission toward the Galactic Center, Astrophys. J. **819**, 44 (2016).

[16] M. Ackermann *et al.* (Fermi-LAT Collaboration), The Fermi Galactic Center GeV excess and implications for dark matter, Astrophys. J. **840**, 43 (2017).

[17] E. Charles *et al.* (Fermi-LAT Collaboration), Sensitivity projections for dark matter searches with the Fermi large area telescope, Phys. Rep. **636**, 1 (2016).

[18] Y. Zhao, X.-J. Bi, P.-F. Yin, and X. Zhang, Constraint on the velocity dependent dark matter annihilation cross section from gamma-ray and kinematic observations of ultrafaint dwarf galaxies, Phys. Rev. D **97**, 063013 (2018).

[19] S. Hoof, A. Geringer-Sameth, and R. Trotta, A global analysis of dark matter signals from 27 dwarf spheroidal galaxies using 11 years of Fermi-LAT observations, J. Cosmol. Astropart. Phys. 02 (2020) 012.

[20] B.-Q. Lu, Y.-L. Wu, W.-H. Zhang, and Y.-F. Zhou, Constraints on the Sommerfeld-enhanced dark matter annihilation from the gamma rays of subhalos and dwarf galaxies, J. Cosmol. Astropart. Phys. 04 (2018) 035.

[21] M. Petac, P. Ullio, and M. Valli, On velocity-dependent dark matter annihilations in dwarf satellites, J. Cosmol. Astropart. Phys. 12 (2018) 039.

[22] S. Ando and K. Ishiwata, Sommerfeld-enhanced dark matter searches with dwarf spheroidal galaxies, Phys. Rev. D **104**, 023016 (2021).

[23] Y. Zhao, X.-J. Bi, S.-J. Lin, and P.-F. Yin, Determination of dark matter distribution in Ursa Major III and constraints on dark matter annihilation, Chin. Phys. C **48**, 115112 (2024).

[24] M. Pospelov, A. Ritz, and M. B. Voloshin, Secluded WIMP dark matter, Phys. Lett. B **662**, 53 (2008).

[25] M. Pospelov and A. Ritz, Astrophysical signatures of secluded dark matter, Phys. Lett. B **671**, 391 (2009).

[26] T. Gherghetta, B. von Harling, A. D. Medina, M. A. Schmidt, and T. Trott, SUSY implications from WIMP annihilation into scalars at the Galactic Center, Phys. Rev. D **91**, 105004 (2015).

[27] B. Holdom, Searching for ϵ charges and a new U(1), Phys. Lett. B **178**, 65 (1986).

[28] S. P. Martin, A supersymmetry primer, Adv. Ser. Dir. High Energy Phys. **18**, 1 (1998).

[29] B. Batell, M. Pospelov, A. Ritz, and Y. Shang, Solar gamma rays powered by secluded dark matter, Phys. Rev. D **81**, 075004 (2010).

[30] N. F. Bell, J. B. Dent, and I. W. Sanderson, Solar gamma ray constraints on dark matter annihilation to secluded mediators, Phys. Rev. D **104**, 023024 (2021).

[31] M. Reece and L.-T. Wang, Searching for the light dark gauge boson in GeV-scale experiments, J. High Energy Phys. 07 (2009) 051.

[32] D. E. Morrissey and A. P. Spray, New limits on light hidden sectors from fixed-target experiments, J. High Energy Phys. 06 (2014) 083.

[33] G. Aad *et al.* (ATLAS Collaboration), Search for massive, long-lived particles using multitrack displaced vertices or displaced lepton pairs in pp collisions at $\sqrt{s} = 8$ TeV with the ATLAS detector, Phys. Rev. D **92**, 072004 (2015).

[34] G. Aad *et al.* (ATLAS Collaboration), Search for light long-lived neutral particles from Higgs boson decays via vector-boson-fusion production from pp collisions at $\sqrt{s} = 13$ TeV with the ATLAS detector, Eur. Phys. J. C **84**, 719 (2024).

[35] P. Schuster, N. Toro, and I. Yavin, Terrestrial and solar limits on long-lived particles in a dark sector, Phys. Rev. D **81**, 016002 (2010).

[36] R. K. Leane, K. C. Y. Ng, and J. F. Beacom, Powerful solar signatures of long-lived dark mediators, Phys. Rev. D **95**, 123016 (2017).

[37] M. Cermeño and M. A. Pérez-García, Gamma rays from dark mediators in white dwarfs, Phys. Rev. D **98**, 063002 (2018).
[38] M. Andrade, J. Fagiani, C. Siqueira, V. de Souza, and A. Viana, Prospects for the detection of dark matter with long-lived mediators in the sun using the southern wide-field gamma-ray observatory, J. Cosmol. Astropart. Phys. 01 (2025) 012.
[39] A. Albert *et al.* (HAWC Collaboration), Constraints on spin-dependent dark matter scattering with long-lived mediators from TeV observations of the sun with HAWC, Phys. Rev. D **98**, 123012 (2018).
[40] C. Arina, M. Backović, J. Heisig, and M. Lucente, Solar γ rays as a complementary probe of dark matter, Phys. Rev. D **96**, 063010 (2017).
[41] C. Niblaeus, A. Beniwal, and J. Edsjo, Neutrinos and gamma rays from long-lived mediator decays in the Sun, J. Cosmol. Astropart. Phys. 11 (2019) 011.
[42] N. F. Bell, G. Busoni, and S. Robles, Capture of leptophilic dark matter in neutron stars, J. Cosmol. Astropart. Phys. 06 (2019) 054.
[43] B. Dasgupta, A. Gupta, and A. Ray, Dark matter capture in celestial objects: Light mediators, self-interactions, and complementarity with direct detection, J. Cosmol. Astropart. Phys. 10 (2020) 023.
[44] I. Z. Rothstein, T. Schwetz, and J. Zupan, Phenomenology of dark matter annihilation into a long-lived intermediate state, J. Cosmol. Astropart. Phys. 07 (2009) 018.
[45] N. Arkani-Hamed, D. P. Finkbeiner, T. R. Slatyer, and N. Weiner, A theory of dark matter, Phys. Rev. D **79**, 015014 (2009).
[46] D. Kim, J.-C. Park, and S. Shin, Dark matter "transporting" mechanism explaining positron excesses, J. High Energy Phys. 04 (2018) 093.
[47] R. K. Leane and T. Linden, First analysis of Jupiter in gamma rays and a new search for dark matter, Phys. Rev. Lett. **131**, 071001 (2023).
[48] L. Li and J. Fan, Jupiter missions as probes of dark matter, J. High Energy Phys. 10 (2022) 186.
[49] J. L. Feng, J. Smolinsky, and P. Tanedo, Dark photons from the center of the earth: Smoking-gun signals of dark matter, Phys. Rev. D **93**, 015014 (2016); **96**, 099901(E) (2017).
[50] R. K. Leane, T. Linden, P. Mukhopadhyay, and N. Toro, Celestial-body focused dark matter annihilation throughout the galaxy, Phys. Rev. D **103**, 075030 (2021).
[51] P. Bhattacharjee, F. Calore, and P. D. Serpico, Gamma-ray flux limits from brown dwarfs: Implications for dark matter annihilating into long-lived mediators, Phys. Rev. D **107**, 043012 (2023).
[52] M. Beneke, S. Lederer, and K. Urban, Sommerfeld enhancement of resonant dark matter annihilation, Phys. Lett. B **839**, 137773 (2023).
[53] W. Wang, W.-L. Xu, J. M. Yang, B. Zhu, and R. Zhu, Sommerfeld enhancement for puffy self-interacting dark matter, J. High Energy Phys. 01 (2024) 114.
[54] M. Phoroutan-Mehr and H.-B. Yu, Relaxing constraints on dark matter annihilation near the supermassive black hole in M87, arXiv:2411.18751.
[55] A. G. Moskowitz and M. G. Walker, Stellar density profiles of dwarf spheroidal galaxies, Astrophys. J. **892**, 27 (2020).
[56] A. W. McConnachie, The observed properties of dwarf galaxies in and around the local group, Astron. J. **144**, 4 (2012).
[57] A. B. Pace, The local volume database: A library of the observed properties of nearby dwarf galaxies and star clusters, arXiv:2411.07424.
[58] A. B. Pace, dSphs Catalog, https://lvd-interactive.streamlit.app/ (2025), Accessed: 2025-05-02.
[59] S. Abdollahi *et al.* (Fermi-LAT Collaboration), Incremental Fermi large area telescope fourth source catalog, Astrophys. J. Suppl. Ser. **260**, 53 (2022).
[60] W. A. Rolke, A. M. Lopez, and J. Conrad, Limits and confidence intervals in the presence of nuisance parameters, Nucl. Instrum. Methods Phys. Res., Sect. A **551**, 493 (2005).
[61] R. R. Muñoz, P. Côté, F. A. Santana, M. Geha, J. D. Simon, G. A. Oyarzún, P. B. Stetson, and S. G. Djorgovski, A megacam survey of outer halo satellites. III. Photometric and structural parameters, Astrophys. J. **860**, 66 (2018).
[62] Z. Bogorad, P. Graham, and H. Ramani, Constraints on long-ranged interactions between dark matter and the standard model, J. Cosmol. Astropart. Phys. 04 (2025) 006.
[63] N. Bernal, J. Martín-Albo, and S. Palomares-Ruiz, A novel way of constraining WIMPs annihilations in the Sun: MeV neutrinos, J. Cosmol. Astropart. Phys. 08 (2013) 011.
[64] A. Bottino, G. Fiorentini, N. Fornengo, B. Ricci, S. Scopel, and F. L. Villante, Does solar physics provide constraints to weakly interacting massive particles?, Phys. Rev. D **66**, 053005 (2002).
[65] R. Garani and S. Palomares-Ruiz, Dark matter in the Sun: Scattering off electrons vs nucleons, J. Cosmol. Astropart. Phys. 05 (2017) 007.
[66] R. K. Leane and J. Smirnov, Exoplanets as Sub-GeV dark matter detectors, Phys. Rev. Lett. **126**, 161101 (2021).
[67] P. Bhattacharjee, D. Choudhury, K. Das, D. K. Ghosh, and P. Majumdar, Gamma-ray and synchrotron radiation from dark matter annihilations in ultra-faint dwarf galaxies, J. Cosmol. Astropart. Phys. 06 (2021) 041.
[68] J. F. Navarro, C. S. Frenk, and S. D. M. White, The structure of cold dark matter halos, Astrophys. J. **462**, 563 (1996).
[69] J. F. Navarro, C. S. Frenk, and S. D. M. White, A universal density profile from hierarchical clustering, Astrophys. J. **490**, 493 (1997).
[70] A. Geringer-Sameth, S. M. Koushiappas, and M. Walker, Dwarf galaxy annihilation and decay emission profiles for dark matter experiments, Astrophys. J. **801**, 74 (2015).
[71] X.-S. Hu, B.-Y. Zhu, T.-C. Liu, and Y.-F. Liang, Constraints on the annihilation of heavy dark matter in dwarf spheroidal galaxies with gamma-ray observations, Phys. Rev. D **109**, 063036 (2024).
[72] F. Calore, M. Cirelli, L. Derome, Y. Genolini, D. Maurin, P. Salati, and P. D. Serpico, AMS-02 antiprotons and dark matter: Trimmed hints and robust bounds, SciPost Phys. **12**, 163 (2022).

[73] Z. Cao *et al.* (LHAASO Collaboration), Constraints on ultraheavy dark matter properties from dwarf spheroidal galaxies with LHAASO observations, Phys. Rev. Lett. **133**, 061001 (2024).
[74] A. Acharyya *et al.*, An indirect search for dark matter with a combined analysis of dwarf spheroidal galaxies from VERITAS, arXiv:2407.16518.
[75] N. W. Evans, J. L. Sanders, and A. Geringer-Sameth, Simple *J*-factors and *D*-factors for indirect dark matter detection, Phys. Rev. D **93**, 103512 (2016).
[76] J. Bramante, A. Delgado, and A. Martin, Multiscatter stellar capture of dark matter, Phys. Rev. D **96**, 063002 (2017).
[77] C. Ilie, J. Pilawa, and S. Zhang, Comment on "Multiscatter stellar capture of dark matter", Phys. Rev. D **102**, 048301 (2020).
[78] R. Garani and S. Palomares-Ruiz, Evaporation of dark matter from celestial bodies, J. Cosmol. Astropart. Phys. 05 (2022) 042.
[79] A. Gould, Weakly interacting massive particle distribution in and evaporation from the Sun, Astrophys. J. **321**, 560 (1987).
[80] G. Busoni, A. De Simone, and W.-C. Huang, On the minimum dark matter mass testable by neutrinos from the Sun, J. Cosmol. Astropart. Phys. 07 (2013) 010.
[81] S. Gori, S. Profumo, and B. Shakya, Wobbly dark matter signals at Cherenkov telescopes from long lived mediator decays, Phys. Rev. Lett. **122**, 191103 (2019).
[82] F. D'Eramo and S. Profumo, Sub-GeV dark matter shining at future MeV γ -ray telescopes, Phys. Rev. Lett. **121**, 071101 (2018).
[83] A. Ibarra, S. Lopez Gehler, and M. Pato, Dark matter constraints from box-shaped γ-ray features, J. Cosmol. Astropart. Phys. 07 (2012) 043.
[84] R. K. Leane and J. Tong, Optimal celestial bodies for dark matter detection, J. Cosmol. Astropart. Phys. 12 (2024) 031.
[85] W. Hofmann and R. Zanin, The Cherenkov telescope array, arXiv:2305.12888.
[86] A. Sommerfeld, Über die Beugung und Bremsung der Elektronen, Ann. Phys. (Berlin) **403**, 257 (1931).
[87] K. K. Boddy, J. Kumar, L. E. Strigari, and M.-Y. Wang, Sommerfeld-enhanced *J*-factors for dwarf spheroidal galaxies, Phys. Rev. D **95**, 123008 (2017).
[88] Z.-P. Liu, Y.-L. Wu, and Y.-F. Zhou, Sommerfeld enhancements with vector, scalar and pseudoscalar force-carriers, Phys. Rev. D **88**, 096008 (2013).
[89] B. Dasgupta and R. Laha, Neutrinos in IceCube/KM3NeT as probes of dark matter substructures in galaxy clusters, Phys. Rev. D **86**, 093001 (2012).
[90] M. Du, R. Fang, Z. Liu, and V. Q. Tran, Enhanced long-lived dark photon signals at lifetime frontier detectors, Phys. Rev. D **105**, 055012 (2022).
[91] T. A. Chowdhury and S. Nasri, The Sommerfeld enhancement in the scotogenic model with large electroweak scalar multiplets, J. Cosmol. Astropart. Phys. 01 (2017) 041.
[92] N. F. Bell, M. J. Dolan, A. Ghosh, and M. Virgato, Neutrino portals to MeV WIMPs with s-channel mediators, Phys. Rev. D **111**, 055020 (2025).
[93] J. Hisano, S. Matsumoto, M. M. Nojiri, and O. Saito, Non-perturbative effect on dark matter annihilation and gamma ray signature from galactic center, Phys. Rev. D **71**, 063528 (2005).
[94] S. Biondini and M. Laine, Thermal dark matter co-annihilating with a strongly interacting scalar, J. High Energy Phys. 04 (2018) 072.
[95] J. Liu, N. Weiner, and W. Xue, Signals of a light dark force in the Galactic Center, J. High Energy Phys. 08 (2015) 050.
[96] S. Cassel, Sommerfeld factor for arbitrary partial wave processes, J. Phys. G **37**, 105009 (2010).
[97] J. L. Feng, M. Kaplinghat, and H.-B. Yu, Sommerfeld enhancements for thermal relic dark matter, Phys. Rev. D **82**, 083525 (2010).
[98] S. Mashchenko, H. M. P. Couchman, and A. Sills, Modeling star formation in dwarf spheroidal galaxies: A case for extended dark matter halos, Astrophys. J. **624**, 726 (2005).
[99] T. R. Slatyer, The Sommerfeld enhancement for dark matter with an excited state, J. Cosmol. Astropart. Phys. 02 (2010) 028.
[100] S. Acevedo and A. R. Zerwekh, Sommerfeld enhancement for vector dark matter in the fundamental representation of SU(2)_L, arXiv:2401.13389.
[101] M. Lattanzi and J. I. Silk, Can the WIMP annihilation boost factor be boosted by the Sommerfeld enhancement?, Phys. Rev. D **79**, 083523 (2009).
[102] J. Hisano, S. Matsumoto, and M. M. Nojiri, Explosive dark matter annihilation, Phys. Rev. Lett. **92**, 031303 (2004).
[103] R. Agnese *et al.* (SuperCDMS Collaboration), Results from the super cryogenic dark matter search experiment at soudan, Phys. Rev. Lett. **120**, 061802 (2018).
[104] C. Amole *et al.* (PICO Collaboration), Dark matter search results from the complete exposure of the PICO-60 C_3F_8 bubble chamber, Phys. Rev. D **100**, 022001 (2019).
[105] R. Ajaj *et al.* (DEAP Collaboration), Search for dark matter with a 231-day exposure of liquid argon using DEAP-3600 at SNOLAB, Phys. Rev. D **100**, 022004 (2019).
[106] J. F. Acevedo, R. K. Leane, and L. Santos-Olmsted, Milky Way white dwarfs as sub-GeV to multi-TeV dark matter detectors, J. Cosmol. Astropart. Phys. 03 (2024) 042.
[107] A. Acharyya *et al.* (VERITAS Collaboration), Indirect search for dark matter with a combined analysis of dwarf spheroidal galaxies from VERITAS, Phys. Rev. D **110**, 063034 (2024).
[108] J. Aalbers *et al.* (LZ Collaboration), First dark matter search results from the LUX-ZEPLIN (LZ) experiment, Phys. Rev. Lett. **131**, 041002 (2023).
[109] Z. Bo *et al.* (PandaX Collaboration), Dark matter search results from 1.54 Tonne Year exposure of PandaX-4T, Phys. Rev. Lett. **134**, 011805 (2025).
[110] K. K. Rogers, C. Dvorkin, and H. V. Peiris, Limits on the light dark matter–proton cross section from cosmic large-scale structure, Phys. Rev. Lett. **128**, 171301 (2022).
[111] E. O. Nadler, V. Gluscevic, K. K. Boddy, and R. H. Wechsler, Constraints on dark matter microphysics from the Milky Way satellite population, Astrophys. J. Lett. **878**, 32 (2019).
[112] K. Maamari, V. Gluscevic, K. K. Boddy, E. O. Nadler, and R. H. Wechsler, Bounds on velocity-dependent dark

matter-proton scattering from Milky Way satellite abundance, Astrophys. J. Lett. **907**, L46 (2021).

[113] E. O. Nadler *et al.* (DES Collaboration), Milky Way satellite census. III. Constraints on dark matter properties from observations of Milky Way satellite galaxies, Phys. Rev. Lett. **126**, 091101 (2021).

[114] V. Gluscevic and K. K. Boddy, Constraints on scattering of keV–TeV dark matter with protons in the early Universe, Phys. Rev. Lett. **121**, 081301 (2018).

[115] K. K. Boddy and V. Gluscevic, First cosmological constraint on the effective theory of dark matter-proton interactions, Phys. Rev. D **98**, 083510 (2018).